AUTOMATED LEFT VENTRICLE SEGMENTATION IN 2-D LGE-MRI

Tanja Kurzendorfer[1], *Alexander Brost*[2], *Christoph Forman*[3] *and Andreas Maier*[1]

[1]Pattern Recognition Lab, Friedrich-Alexander-University Erlangen-Nuremberg, Erlangen, Germany
[2]Siemens Healthcare GmbH, Forchheim, Germany
[3]Siemens Healthcare GmbH, Erlangen, Germany

ABSTRACT

For electrophysiology procedures, obtaining the information of scar within the left ventricle is very important for diagnosis, therapy planning and patient prognosis. The clinical gold standard to visualize scar is late-gadolinium-enhanced-MRI (LGE-MRI). The viability assessment of the myocardium often requires the prior segmentation of the left ventricle (LV). To overcome this problem, we propose an approach for fully automatic LV segmentation in 2-D LGE-MRI. First, the LV is automatically detected using circular Hough transforms. Second, the blood pool is approximated by applying a morphological active contours approach. The refinement of the endo- and epicardial contours is performed in polar space, considering the edge information and scar distribution. The proposed method was evaluated on 26 clinical LGE-MRI data sets. This comparison resulted in a Dice coefficient of 0.85 ± 0.06 for the endocardium and 0.84 ± 0.06 for the epicardium.

***Index Terms*—** Heart; Magnetic Resonance Imaging (MRI); Image Segmentation

1. INTRODUCTION

For electrophysiology procedures, obtaining the information of scar within the myocardium is important, but remains a challenge. The quantification of the myocardial infarction is needed for diagnosis, therapy planning and patient prognosis. The clinical gold standard to visualize scar is late-gadolinium-enhanced magnetic resonance imaging (LGE-MRI) [1]. These images are acquired 10 to 20 minutes after contrast agent injection, of a gadolinium based contrast agent. Areas of myocardial infarction will be enhanced because of the contrast agent accumulation in the scar tissue [2].
The viability assessment of the myocardium often requires the prior segmentation of the myocardial contours [3]. In clinical routine manual outlining of the left ventricles myocardium is the current practice. However, the manual delineation of the left ventricles myocardium is complex, tedious, time consuming and prone to intra- and inter-observer variability. The main challenge of left ventricle (LV) segmentation in LGE-MRI is the non-homogeneous intensity distribution within the myocardium, resulting from the different contrast agent accumulation in the damaged tissue. Therefore, the challenge of LGE-MRI segmentation lies in the border delineation. Hence, most segmentation methods most often rely on the registration of the LGE-MRI to anatomical MRI scans or shape priors [4, 5, 6, 7]. The segmented contours from the anatomical scan are propagated to the LGE-MRI for segmentation. However, this registration is challenging. Between both scans, the global position of the heart may have changed due to patient movement or different breath-hold levels. Furthermore, the cardiac phases may not precisely fit to the LGE-MRI images. Even though these shifts appear minor, they can lead to a significant error in the quantification of myocardial scar.
To overcome these issues, we propose a fully automatic left ventricle segmentation solely using 2-D short axis (SA) LGE-MRI data.

2. METHODS

Our approach consists of four major steps. First, the left ventricle is detected in the middle slice using circular Hough transforms. Second, the blood pool is segmented by applying a morphological active contours approach without edges (MACWE). In the third step, the endocardial contour is refined in polar space using the edge and scar information and applying a minimal cost path search (MCP). Fourth, the epicardium is extracted considering the edge information and the endocardial contour. Fig. 1 provides an overview of the segmentation pipeline. These steps are detailed in the next subsections.

2.1. Left Ventricle Detection

The automatic initialization of the left ventricle is an important part, in order to reduce the user interaction. The left ventricle is detected in the middle slice of the 2-D SA LGE-MRI stack. Therefore, circular Hough transforms are applied to approximate the location of the left ventricle [8]. First, the center slice is filtered with a Canny edge detector, to extract all edges from the images [9]. Gaussian smoothing with a standard deviation of $\sigma = 1.5$ is applied. The radius r for the circular Hough transform is in range of

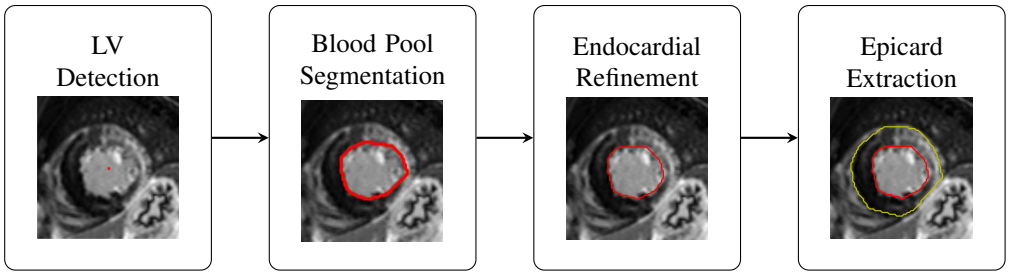

Fig. 1. Overview of the left ventricle segmentation pipeline in 2-D LGE-MRI. First, the left ventricle is detected using circular Hough transforms. In the next step, the blood pool is segmented by applying a morphological active contours approach without edges. In the third step, the endocardial border is refined in polar space. In the final step, the epicardial contour is extracted considering the endocardial contour and the edge information.

$r = \{17, 19, 21, ..., 33, 35\}$ mm. This range was defined using anatomical heart information as reported in literature [10]. The center point of the LV is then propagated to the succeeding slices, which is detailed in Subsection 2.3.

2.2. Blood Pool Segmentation

Having the rough location of the left ventricle, the center point from the LV detection is used as initialization for a morphological active contours approach without edges [11]. The MACWE algorithm does not need well defined borders, as the stopping of the curve evolution is not dependent on edges, instead it uses image statistics from the inside as well as from the outside of the contour. Furthermore, it is less sensitive to initial configuration and to model parameters. The difference to standard active contour approaches without edges is, that the partial differential equations are replaced by morphological operations, as they are less computational expensive and more stable. The energy functional for the segmentation takes the content of the interior and exterior areas of the contour $\mathbf{C}$ into account. The functional for the contour $\mathbf{C}$ is dependent on the image slice $\mathbf{I}$ and defined by

$$F(c_1, c_2, \mathbf{C}) = \mu \cdot L(\mathbf{C}) + \nu \cdot A(\mathbf{C}) + \lambda_1 \int_{\Omega} ||\mathbf{I}(x) - c_1||dx + \lambda_2 \int_{\overline{\Omega}} ||\mathbf{I}(x) - c_2||dx, \quad (1)$$

where the non-negative parameters $\mu = 1$, $\nu = 1$, $\lambda_1 = 1$ and $\lambda_2 = 2 \in \mathbb{R}$ control the strength of each term, L denotes the length of the contour $\mathbf{C}$ and A the area of the contour $\mathbf{C}$. For a fixed contour, c_1 and c_2 are the mean intensity values of the area inside Ω and outside $\overline{\Omega}$ of the contour $\mathbf{C}$. Therefore, an implicit version of the functional F of Equation 1 can be defined [11]. For the starting of the contour evolution, a circle is initialized using the detected center from the LV detection and a radius of 10 pixels. The MACWE is stopped after 15 iterations, heuristically chosen. See the second box of Fig. 1 for an example result from the MACWE evolution.

2.3. Endocardial Contour Refinement

After the blood pool approximation of the left ventricle, the contour $\mathbf{C}$ is used for the refinement of the endocardial border. As the rough outline of the LV is known, the image $\mathbf{I}$ is cropped around the region of interest, to perform further image processing steps on the cropped image.
The polar image is calculated, where the origin of the polar image corresponds to the center of the blood pool. Through this mapping the Cartesian coordinates (x, y) are converted to polar coordinates (r, ρ). The maximum radius is selected, to cover all potential myocardium boundaries. The estimated contours $\mathbf{C}$ from the blood pool are also converted to polar coordinates and used to refine the endocardial boundary. Fig. 2 (a) depicts an example of the polar image and the converted contours. In the polar image the edge information is extracted by applying the Canny edge detection [9]. To extract minor edges, a Gaussian smoothing with a standard deviation of $\sigma = 1.5$ is used, see Fig. 2 (b) for an example. In addition, the mean intensity μ_{bp} and the standard deviation σ_{bp} of the blood pool are estimated, using the intensity values inside the contour obtained from the MACWE approach. In the next step, all pixels that are greater than the mean intensity μ_{bp} plus the standard deviation σ_{bp} are defined as potential myocardial scar and labeled with 1, the non-scar pixels are marked with 0. All pixels with increasing radius after the potential scar candidates are labeled with 1, resulting in a scar map, as visualized in Fig. 2 (c). The scar map is combined with the edge image, which derives the cost array for the minimal cost path search, as shown in Fig. 2 (d). Six equally distributed points are selected from the converted blood pool contours $\mathbf{C}$ and the minimal cost path search is initialized to find the optimal contour [12]. The MCP finds the distance weighted minimal cost path through the cost array. The cost path is calculated as the sum of the costs at each point of the path, where edge pixels have 0 costs and non edge pixels 1. The diagonal versus axial moves are of different length and therefore the path costs are weighted accordingly. The result of the MCP is illustrated in Fig. 2 (e). After the refinement,

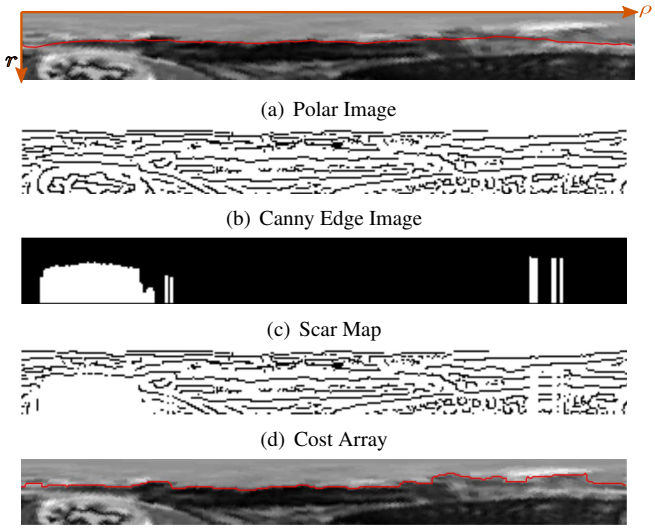

(a) Polar Image

(b) Canny Edge Image

(c) Scar Map

(d) Cost Array

(e) Final Result of MCP

Fig. 2. Final steps of the segmentation pipeline. (a) Polar image with the converted contour points from the blood pool segmentation. (b) Edge image using the Canny edge detection (c) Scar map. (d) The cost array is derived from the edge image and the scar map. (e) Final result of the minimal cost path search.

the contour $\mathbf{C}$ is converted back to Cartesian coordinates. As the result might be frayed and papillary muscles close to the endocardial border may be included, the convex hull is calculated for the estimated points. This assumption is based on the fact that the left ventricles cavity is convex in the SA view. The final contour $\mathbf{C}$ is derived from the smallest convex polygon, as depicted in the third box of Fig. 1. This is based on the fact that the left ventricles cavity is convex in the short axis orientation.
After the first contour is refined, the information of the location of the LV is used for the initialization of the MACWE for the succeeding slices in basal and apical direction. The refinement steps are repeated for every slice. Furthermore, the radius and area of the previous curve are considered for the refinement of the lower and upper slices.

2.4. Epicardial Contour Extraction

For the epicardial contour extraction the previously found endocardial contour points are used. The contour extraction is performed in polar space. As the epicardium has to be greater than the endocardium, the radius is enlarged by $r_{\text{epi}} = 5$. The previously calculated edge image from the endocardial refinement is used. The edges within the endocardial segment are erased. Having the enlarged endocardial contour, the closest edge with increased radius, in a certain margin is searched for. Afterwards, the newly found edge points are converted back to Cartesian coordinates. As the result is frayed, the convex hull is estimated to smooth the contour. The final result for the endocardial and epicardial contour is depicted in the fourth box of Fig. 1.

Segmentation Results

	Endo	Epi	Inter-Obs.
DC	0.85	0.84	0.96
ASD [mm]	2.54	3.32	0.64

Table 1. Quantitative results of the LV segmentation using the Dice coefficient (DC) and the average surface distance (ASD). The results are shown separately for the endocardial (Endo) and epicardial (Epi) contour, as well as the inter observer variability.

3. EVALUATION AND RESULTS

The automatic segmentation of the LV endocardium and epicardium was evaluated on 26 clinical LGE-MRI data sets from individual patients. The inversion recovery LGE-MRI sequences were acquired with a Siemens MAGNETOM Aera 1.5T scanner (Siemens Healthcare GmbH, Erlangen, Germany). The slice thickness was set to 8 mm, with a pixel size of (1.59-2.08 $\times$ 1.59-2.08) mm^2 and the spacing between the slices was set to 10 mm. Each data set contained between 10 and 13 SA slices. The parameters set, were equal for all cases. Gold standard annotations of the LV endo- and epicardium were provided by two clinical experts. Given the gold standard annotations, the Dice coefficient (DC) as a quantitative score of the segmentation quality and the average surface distance (ASD) between the gold standard annotation and the segmentation result are evaluated. In addition, the inter-observer variability between the observers is investigated.
The automatic segmentation of the endocardium resulted in an overlap of 0.85 $\pm$ 0.06. The best segmentation result had a Dice coefficient of 0.94 and the worst a DC of 0.71. For the epicardium, an overall Dice coefficient of 0.84 $\pm$ 0.06 was achieved. The best segmentation of the epicardium yielded a Dice coefficient of 0.95 and the worst a Dice coefficient of 0.72. The inter-observer variability between the two observers resulted in a DC of 0.96 $\pm$ 0.03 for the endocardium and 0.97 $\pm$ 0.03 for the epicardium. The average surface distance had a mean distance of 2.54 mm $\pm$ 1.54 mm for the endocardium and 3.32 mm $\pm$ 1.71 mm for the endocardium. The results are summarized in Table 1. The qualitative results for one data set are presented in Fig. 3.

4. DISCUSSION AND CONCLUSION

The segmentation of the LV endo- and epicardium has been studied in literature, but only a few focused on LGE-MRI data only [5, 13]. The presented work solely uses LGE-MRI for the contour segmentation. In one data set, there was a huge

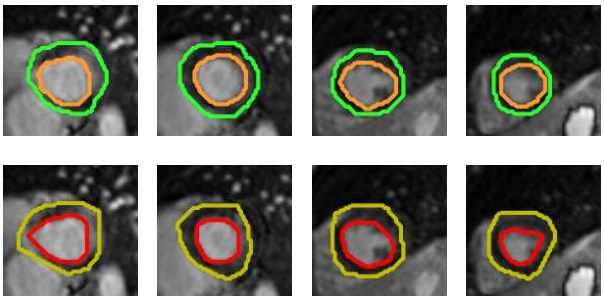

Fig. 3. Qualitative results for one data set from base to apex, with a DC of 0.73. The first row shows the gold standard annotation from the clinical expert. The second row depicts the result from the proposed segmentation pipeline.

equally distributed myocardial scar around the blood pool in the apex. This resulted in the reduced Dice coefficient of 0.71 for the endocardium and 0.72 for the epicardium. Another problem is the delineation of the left ventricular outflow track, therefore larger errors occur in the more basal regions.

In the course of this work an automatic segmentation method for the left ventricle's endo and epicardium has been presented that provides accurate and consistent results using 2-D LGE-MRI. A clear benefit of the presented method is that solely LGE-MRI is used for the segmentation.

Disclaimer: The methods and information presented in this paper are based on research and are not commercially available.

5. REFERENCES

[1] T. Shin, M. Lustig, D. Nishimura, and B. Hu, "Rapid single-breath-hold 3D late gadolinium enhancement cardiac MRI using a stack-of-spirals acquisition," *Journal of Magnetic Resonance Imaging*, vol. 40, no. 6, pp. 1496–1502, December 2014.

[2] Adelina Doltra, Brage Hoyem Amundsen, Rolf Gebker, Eckart Fleck, and Sebastian Kelle, "Emerging Concepts for Myocardial Late Gadolinium Enhancement MRI," *Current Cardiology Reviews*, vol. 9, no. 3, pp. 185–190, August 2013.

[3] Rashed Karim, Pranav Bhagirath, Piet Claus, R James Housden, Zhong Chen, Zahra Karimaghaloo, Hyon-Mok Sohn, Laura Lara Rodríguez, Sergio Vera, Xènia Albà, et al., "Evaluation of state-of-the-art segmentation algorithms for left ventricle infarct from late Gadolinium enhancement MR images," *Medical Image Analysis*, vol. 30, pp. 95–107, May 2016.

[4] Q. Tao, S. Piers, H. Lamb, and R. van der Geest, "Automated Left Ventricle Segmentation in Late Gadolinium-Enhanced MRI for Objective Myocardial Scar Assessment," *Journal of Magnetic Resonance Imaging*, vol. 42, no. 2, pp. 390–399, August 2015.

[5] Xènia Albà, Figueras i Ventura, M Rosa, Karim Lekadir, Catalina Tobon-Gomez, Corné Hoogendoorn, and Alejandro F Frangi, "Automatic Cardiac LV Segmentation in MRI Using Modified Graph Cuts with Smoothness and Interslice Constraints," *Magnetic Resonance in Medicine*, vol. 72, no. 6, pp. 1775–1784, December 2014.

[6] Avan Suinesiaputra, Brett R Cowan, Ahmed O Al-Agamy, Mustafa A Elattar, Nicholas Ayache, Ahmed S Fahmy, Ayman M Khalifa, Pau Medrano-Gracia, Marie-Pierre Jolly, Alan H Kadish, et al., "A collaborative resource to build consensus for automated left ventricular segmentation of cardiac MR images," *Medical Image Analysis*, vol. 18, no. 1, pp. 50–62, January 2014.

[7] Jordan Ringenberg, Makarand Deo, Vijay Devabhaktuni, David Filgueiras-Rama, Gonzalo Pizarro, Borja Ibañez, Omer Berenfeld, Pamela Boyers, and Jeffrey Gold, "Automated segmentation and reconstruction of patient-specific cardiac anatomy and pathology from in vivo MRI," *Measurement Science and Technology*, vol. 23, no. 12, pp. 125405, 2012.

[8] Richard O Duda and Peter E Hart, "Use of the Hough transformation to detect lines and curves in pictures," *Communications of the ACM*, vol. 15, no. 1, pp. 11–15, January 1972.

[9] John Canny, "A Computational Approach to Edge Detection," *IEEE Transactions on Pattern Analysis and Machine Intelligence*, , no. 6, pp. 679–698, November 1986.

[10] Roberto M Lang, Michelle Bierig, Richard B Devereux, Frank A Flachskampf, Elyse Foster, Patricia A Pellikka, Michael H Picard, Mary J Roman, James Seward, Jack Shanewise, et al., "Recommendations for chamber quantification," *European Heart Journal-Cardiovascular Imaging*, vol. 7, no. 2, pp. 79–108, February 2006.

[11] Pablo Marquez-Neila, Luis Baumela, and Luis Alvarez, "A morphological approach to curvature-based evolution of curves and surfaces," *IEEE Transactions on Pattern Analysis and Machine Intelligence*, vol. 36, no. 1, pp. 2–17, January 2014.

[12] Edsger Dijkstra, "A Note on Two Problems in Connexion with Graphs," *Numerische Mathematik*, vol. 1, no. 1, pp. 269–271, 1959.

[13] Jenny Folkesson, Eigil Samset, Raymond Y Kwong, and Carl-Fredrik Westin, "Unifying Statistical Classification and Geodesic Active Regions for Segmentation of Cardiac MRI," *IEEE Transactions on Information Technology in Biomedicine*, vol. 12, no. 3, pp. 328–334, May 2008.